ADVANCED MATERIALS
www.advmat.de

# Robust Mix-Charged Polyzwitterionic Hydrogels for Ultra-Efficient Atmospheric Water Harvesting and Evaporative Cooling

*Xuanxuan Du, Zhiheng Xie, Hanchao Zhang, Shoukun Jiang, Xing Su, and Jintu Fan**

**Atmospheric water harvesting (AWH) presents great potential in addressing the increasing global challenges in freshwater and energy supply, especially in arid and semi-arid regions. The recent AWH materials focus primarily on maximizing water uptake, while conventional approaches prioritize hygroscopicity at the expense of mechanical integrity, which severely limits their applicability in real-world scenarios. In this study, a novel tunable hygroscopic mix-charged polyzwitterionic hydrogel (THMPH) is reported that achieves dual excellence in outstanding moisture absorbency and mechanical robustness. Owing to the broad ionic crosslink's degree enabling the rigid skeletal framework and energy-dissipative sacrificial networks, THMPH exhibits more than 200 times higher mechanical ductility (225 kPa tensile strength retention at 200% mass swelling ratio) in comparison with the commonly-used AWH zwitterionic polybetaine. The optimized topological structure coupled with improved lithium chloride binding affinity results in excellent water uptake (2.9 g $g^{-1}$ at 25 °C, 70% RH). When THMPH is used for daytime photovoltaic panel cooling, it can provide a 15 °C temperature reduction of a PV panel under 1 kW $m^{-2}$ solar irradiation, resulting in a 7.33% increase in solar energy conversion efficiency. This hydrogel design paradigm, synergizing superior hygroscopicity with exceptional mechanical robustness, demonstrates significant potential for advancing practical applications.**

## 1. Introduction

The growth of the global population and expansion of energy-intensive industries have increased the pressure on the supply of freshwater and energy. For now, over 6 billion population still faces difficulties in accessing freshwater and/or reliable electricity, and this number is projected to exceed 50 billion by 2050.[1–3] Sorption-based atmospheric water harvesting (SAWH) through extracting freshwater from atmospheric water vapor, estimated at 12 900 trillion kilograms,[4,5] offers a great potential solution, especially in arid and semi-arid regions. The harvested water can also be used for evaporative cooling of photovoltaic (PV) panels, thereby significantly improving the energy conversion efficiency of PV electricity generation,[6–8] which is to become a primary global electricity source by 2027.[9]

In recent years, a variety of SAWH materials have been developed, including metal–organic frameworks (MOF),[10–13] covalent organic frameworks (COF),[14,15] zeolites,[16–18] activated carbon,[19] silica gel,[20,21] hygroscopic salts,[22–24] natural materials,[25] salt-based composites[26,27] and salt-based hydrogels.[28,8,29,30] Among these, salt–based hydrogels are favored for their excellent adsorption kinetics and water retention properties. While existing research efforts have resulted in a significant enhancement in the water uptake rates of synthesized hydrogels through optimizing polymer composition and hydrogel structures,[31–34] poor mechanical performance, viz. tensile strength, fracture toughness, and fatigue resistance, remains to be the bottleneck for their wide application. Specifically, due to network dilution and weakened interactions between polymer chains after water absorption, the mechanical properties of hydrogels degrade significantly.[35] Some attempts have been made to modify the monomer and crosslinker concentrations during synthesis to enhance the mechanical strength of the hydrogels, but the improvements have been limited.[36,37] Moreover, strengthening the mechanical properties often restricts the swelling capacity, resulting in a significant reduction in hygroscopicity. Incorporation of nanomaterials such as carbon nanotubes and graphene oxide into hydrogel matrices can improve

X. Du, H. Zhang, S. Jiang, X. Su, J. Fan
School of Fashion and Textiles
The Hong Kong Polytechnic University
Hong Kong 00852, China
E-mail: jin-tu.fan@polyu.edu.hk
Z. Xie
Beijing National Laboratory for Molecular Sciences
Center for Integrated Spectroscopy
College of Chemistry and Molecular Engineering
Peking University
Beijing, Beijing 100871, China

The ORCID identification number(s) for the author(s) of this article can be found under https://doi.org/10.1002/adma.202505279



**DOI: 10.1002/adma.202505279**

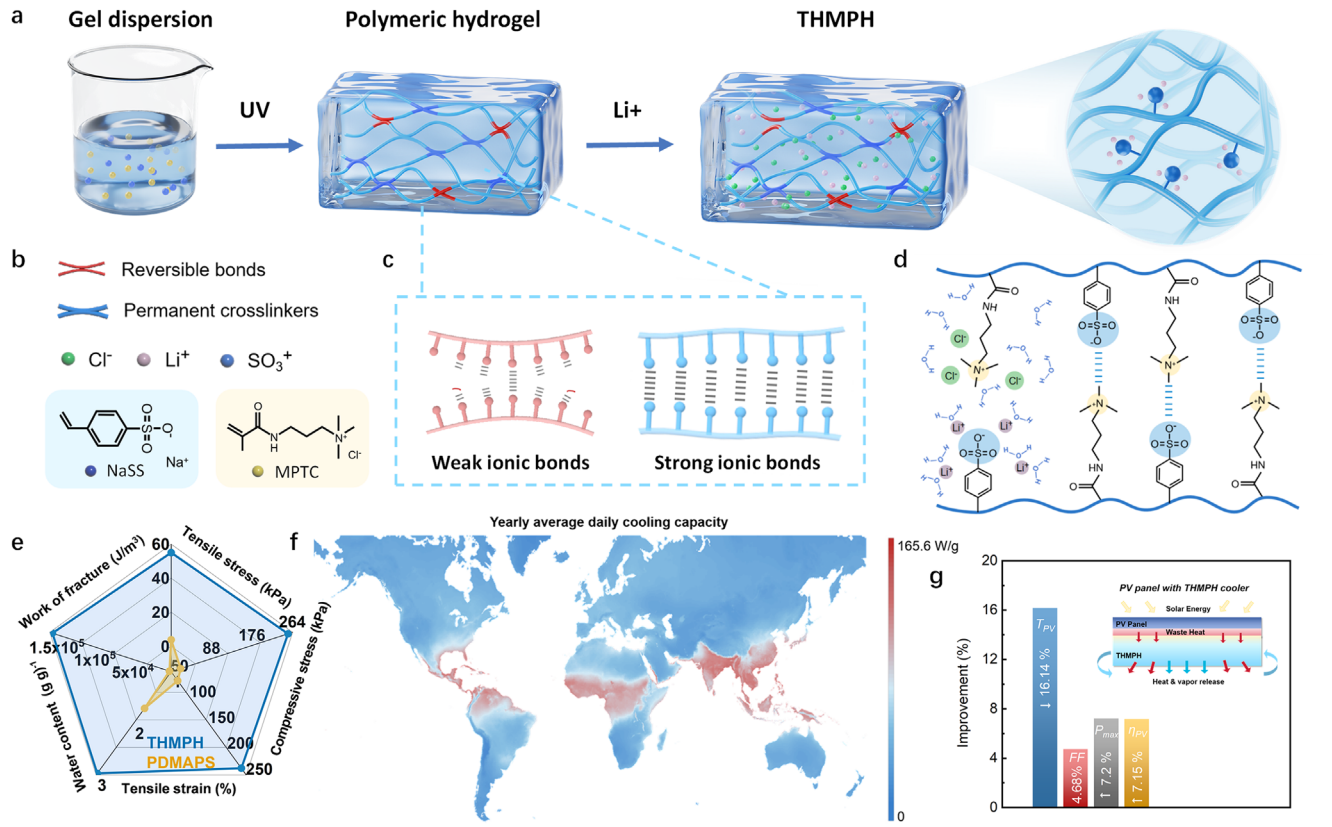


**Figure 1.** Structural design and performance of THMPH. a) Preparation and characterization of THMPH. b) The chemical structures of monomers used in this work. Anionic monomer: Sodium 4-vinylbenzenesulfonate (NaSS); cationic monomer: 3-(methacryloylamino)propyl-trimethylammonium Chloride (MPTC). c) Schematic diagram of strong and weak crosslinked networks within THMPH. d) Weak and strong crosslinked structures. e) Comparison of comprehensive performance between THMPH and PDMAPS. f) The predicted annual average daily cooling performance of THPMH when applied to evaporative cooling is based on humidity, with relative humidity indicated in order from low to high (blue to red). g) Relative electrical improvements of the PV panel cooling module compared to the standalone PV panel.

mechanical performance by reinforcing the structural framework and increasing crosslinking density.[38,39] However, limitations associated with interfacial interactions, dispersion quality, network compatibility, and pore volume may restrict the effective loading capacity of nanomaterials within the hydrogel network, adversely affecting the moisture absorption capacity and rate.[40–43] SAWH hydrogels made of biomass materials have potential due to their inherent hydrophilicity and complex porous structures, but their mechanical strength remains unsatisfactory.[44] The cryogelation method to prepare SAWH hydrogels has led to a moderate improvement in tensile fracture strength compared to the original polymer.[28] However, due to the inherent trade-off between toughness-stiffness conflict in single network hydrogels,[45–47] the extensibility was diminished. Despite considerable research efforts, achieving both superior mechanical performance and excellent water absorbency remains a challenge.

In this study, a generalized strategy was established for developing SAWH that integrates hygroscopicity with mechanical robustness. The novel tunable hygroscopic mix-charged polyzwitterionic hydrogel (THMPH) was synthesized via a simple method (**Figure 1**a,b). By adjusting its monomer composition, the mechanical properties can be altered. Unlike conventional polyampholyte hydrogels relying on uniform ionic crosslinking such as poly-[2-(methacryloyloxy)ethyl]dimethyl-(3-sulfopropyl) ammonium hydroxide (PDMAPS), THMPH features a network structure with multiple crosslinking forms resulted from the complexation of randomly distributed opposite charges in ionic bonds of varying strengths.[48,49] Ionic bonds with dissociation energies exceeding thermal energy but remaining below covalent bond thresholds can sustain mechanical loads during deformation while predominantly fracturing prior to covalent bond rupture, exhibiting weak bond characteristics. In contrast, ionic bonds containing hundreds of ion pairs with dissociation energies surpassing covalent bond levels typically function as structural frameworks supporting hydrogel structure. (Figure 1c).

When water molecules enter into the network, unlike the conventional PDMAPS hydrogel, which undergoes significant expansion due to the extensive dissociation of weakly crosslinked framework formed by sterically hindered side-chain ion pairing, a strong and homogeneous topological network of THMPH consisting of the multilevel ionic crosslinking structure remains intact, preventing excessive swelling. This stability suppresses the self-association of hydrophilic charged side chains, resulting in an increased side chain density. Furthermore, the homogeneous

network structure and highly charged side chain density facilitate more stable loading of hygroscopic salts, laying the foundation for enhanced adsorption kinetics (Figure 1d). Consequently, the water uptake capacity of THMPH achieved up to 2.9 g $g^{-1}$ at 30 °C and 70% relative humidity (RH) (Figure 1e, Table S1, Supporting Information), which ≈1.5 times faster than that of the conventional PDMAPS. Based on its high adsorption performance across a wide range of humidity levels, THMPH-based materials can be applied in water harvesting and evaporative cooling systems (Figure S1, Table S2, Supporting Information), with a predicted daily water harvesting potential of exceeding 3.66 kg $kg^{-1}$ $day^{-1}$ and equivalent evaporative cooling power potential of 100 W $m^{-2}$ in most areas, and up to 591.4 W $m^{-2}$ in high humidity region (Figure 1f). Moreover, by applying the THMPH to cool the PV panel, the maximum power and electrical efficiency were improved by 7.2% and 7.15% relative to the standalone PV panel as shown in Figure 1g. In summary, we have developed a novel strategy for fabricating high-performance SAWH hydrogels without the intrinsic trade-off between hygroscopicity and robustness for addressing the fresh water and energy challenge.

## 2. Results and Discussion

### 2.1. Preparation and Characterization of THMPH

THMPH hydrogels were synthesized via one-step copolymerization of oppositely charged monomers, NaSS for anions and MPTC for cations, in a sodium chloride(NaCl)-containing precursor solution (Figure 1b). Ionic crosslinking density was modulated by NaCl concentration, followed by post-polymerization immersion in lithium chloride(LiCl) solution to embed hygroscopic salts (Figure S2, Supporting Information). Variation of monomer component, charge ratio, and crosslinker content enabled control of hydrophilicity, crosslinking degree, and mechanical properties. (Figure S3, Supporting Information). For comparison purposes, PDMAPS hydrogels were prepared with matched monomer concentration and crosslinking density, incorporating equivalent LiCl loading (Figure S4, Supporting Information). PDMAPS is synthesized from a zwitterionic monomer containing both positively and negatively charged groups in its side chain, whereas THMPH is copolymerized using two distinct monomers carrying positive and negative charges, respectively (Figure S5, Supporting Information).[50] In PDMAPS, zwitterionic DMAPS monomers underwent intra-chain dipole interactions, forming densely crosslinked networks via charge self-association. Salt ions disrupt these interactions through screening effects, triggering anti-polyelectrolyte behavior (swelling/fluidity enhancement). Conversely, THMPH achieved uniform topological networks through randomized ionic associations between discrete anionic and cationic monomers during polymerization, enabling multilevel charge interactions with less localized dipole aggregation.

Structural characterization revealed distinct network architectures. Scanning electron microscopy (SEM) images exhibited a loose mesh structure of THMPH with a uniformly arranged polymer network after moisture absorption and freezing, while PDMAPS displayed dense, hydrophobic self-associated structures (**Figure 2a**). Higher-resolution images further revealed brittle fracture features in PDMAPS, including cracks and fragments due to weak ionic crosslinking (Figure S6, Supporting Information). Conversely, THMPH displayed smooth, intact polymer surfaces, indicative of increased crosslinking and mechanical strength. Figure 2c provided a statistical analysis of the pore areas in the frozen SEM images, showing that THMPH have a larger pore size distribution, with an average pore area of ≈116.1 $\mu m^2$, compared to an average area of 63.9 $\mu m^2$ for PDMAPS. The obvious pore-size differences stem from the distinct degrees of freedom of the polymers' charged moieties. In PDMAPS, self-association constrains network expansion, and the hydrophobic character of these domains further limits water uptake, yielding a low-porosity hydrogel. By contrast, THMPH bears highly mobile positive and negative charges that form ionic cross-links of varying strength across the network, with minimal self-association. Moreover, the dynamic dissociation of weak ionic cross-links in water enlarges network voids without damaging the primary scaffold, thereby with superior water uptake capacity. Density functional theory calculations elucidated molecular crosslinking behavior and pore size difference of two hydrogels by comparing NaSS-MPTC and DMAPS-DMAPS ion pairs (Figure S7, Supporting Information), affected by the steric hindrance. The dissociation energy of two ion pairs suggests the crosslinking stability (Figure S8, Supporting Information), and suggests the different LiCl loading behavior of THMPH and PDMAPS, which aligns with enhanced LiCl retention and leakage resistance post-dehydration in THMPH.

Fourier transform infrared spectrometer (FTIR) analysis identified strengthened ionic crosslinking in THMPH through sulfonate group interactions (S═O peak shift from 1037 to 1046 $cm^{-1}$ upon dehydration). In contrast, dehydrated PDMAPS showed split S═O peaks, reflecting high-density self-associated networks post-dehydration (Figure 2b; Figures S9 and S10, Supporting Information). Notably, LiCl incorporation did not alter this peak position, confirming the structural integrity. All hydrated samples exhibited a broad —OH peak at 3390 $cm^{-1}$, confirming extensive water retention. Common features included —CH stretching vibrations in $CH_2$ (2876 $cm^{-1}$) and $—N^+(CH_3)_3$ (1479 $cm^{-1}$), assigned to hydrocarbon chains and quaternary ammonium groups, respectively. THMPH uniquely displayed benzene ring vibrations at 1009 and 1124 $cm^{-1}$ from NaSS side chains. Thermogravimetric analysis (TGA) confirmed that THMPH showed lower free water loss and higher bound water loss, showed enhanced hygroscopicity, attributed to its elevated LiCl loading. THMPH also demonstrated higher decomposition temperatures, indicative of a stable ionic crosslinked network. Consistent weight loss near 350 °C across dry, unloaded, and LiCl-loaded hydrogels confirmed that water and LiCl incorporation minimally perturbed the polymer matrix (Figure 2d; Figures S11 and S12, Supporting Information). The comparative analysis of LiCl content demonstrates that THMPH exhibits a significantly higher loading capacity (Figure S13, Supporting Information). Meanwhile, rheological tests characterized the crosslinking strength of THMPH and PDMAPS (Figure 2e,f). Both hydrogels exhibited a storage modulus (G′) higher than the loss modulus (G″) across tested temperatures, confirming stable solid-like behavior. THMPH exhibited significantly higher G′ and G″ values than PDMAPS, reflecting its denser network, enhanced

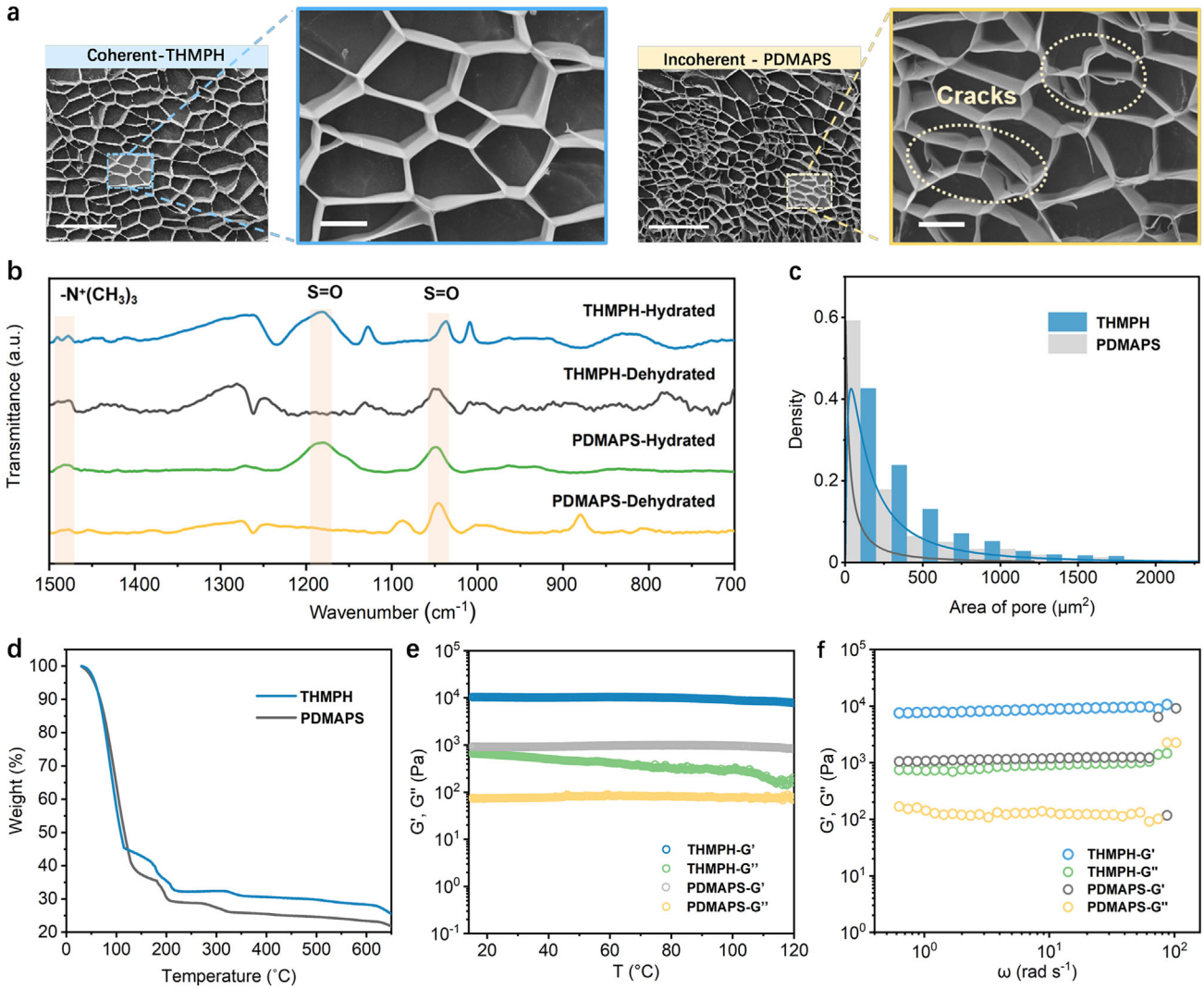


**Figure 2.** Structural characterization of THMPH and PDMAPS. a) Scanning electron microscope (SEM) images of THMPH and PDMAPS with a scale bar of 50 μm. High-magnification images show the polymer microstructure with a scale bar of 10 μm. b) Fourier transform infrared spectrometer (FTIR) characteristic spectra of PDAMPS, THMPH, and THMPH without LiCl loading in the absence and presence of water. c) Statistical results of pore area distribution in SEM images. d) Thermogravimetric analysis (TGA) curves of the two hydrogels in the aqueous state. The red boxes marked the three weight loss intervals. e) Rheological characterization of THMPH and PDMAPS, both tested in water-containing conditions. f) Temperature-dependent rheological tests.

mechanical strength, and superior energy storage capability at equivalent hydration. Repeated tests confirmed consistency (Figure S14, Supporting Information).

### 2.2. Adsorption–Desorption Properties of Hydrogels

The distinct crosslinking structures directly influenced hydrogels swelling behavior of the hydrogels. THMPH and PDMAPS displayed contrasting responses in pure water and in 10% and 50% saturated LiCl solutions (Figures S15 and S16, Supporting Information). THMPH achieved a high swelling ratio (≈8 g $g^{-1}$) in both water and salt solution, attributed to weak crosslink dissociation allowing network expansion, while strong crosslinks ensured structural stability. The slightly reduced swelling in salt solutions likely resulted from external osmotic pressure effects. In contrast, self-associated aggregates of PDMAPS limited swelling (≈3 g $g^{-1}$ in pure water). At 10% saturated LiCl, salt ions dissociated these aggregates, the swelling ratio increased to ≈19 g $g^{-1}$, exhibiting a typical anti-polyelectrolyte effect. However, this expansion of the network compromised mechanical integrity and LiCl leakage due to crosslink loosening. As the salt concentration increases, restricted ion transfer reduced the swelling equilibrium rate of THMPH, further highlighting its instability under high salinity (Figure S17, Supporting Information).

The uniform topological network and high LiCl loading capacity endowed THMPH with superior hygroscopic performance (**Figure 3**a). Specifically, THMPH showed a 40% higher water adsorption rate and twice the desorption rate of PDMAPS

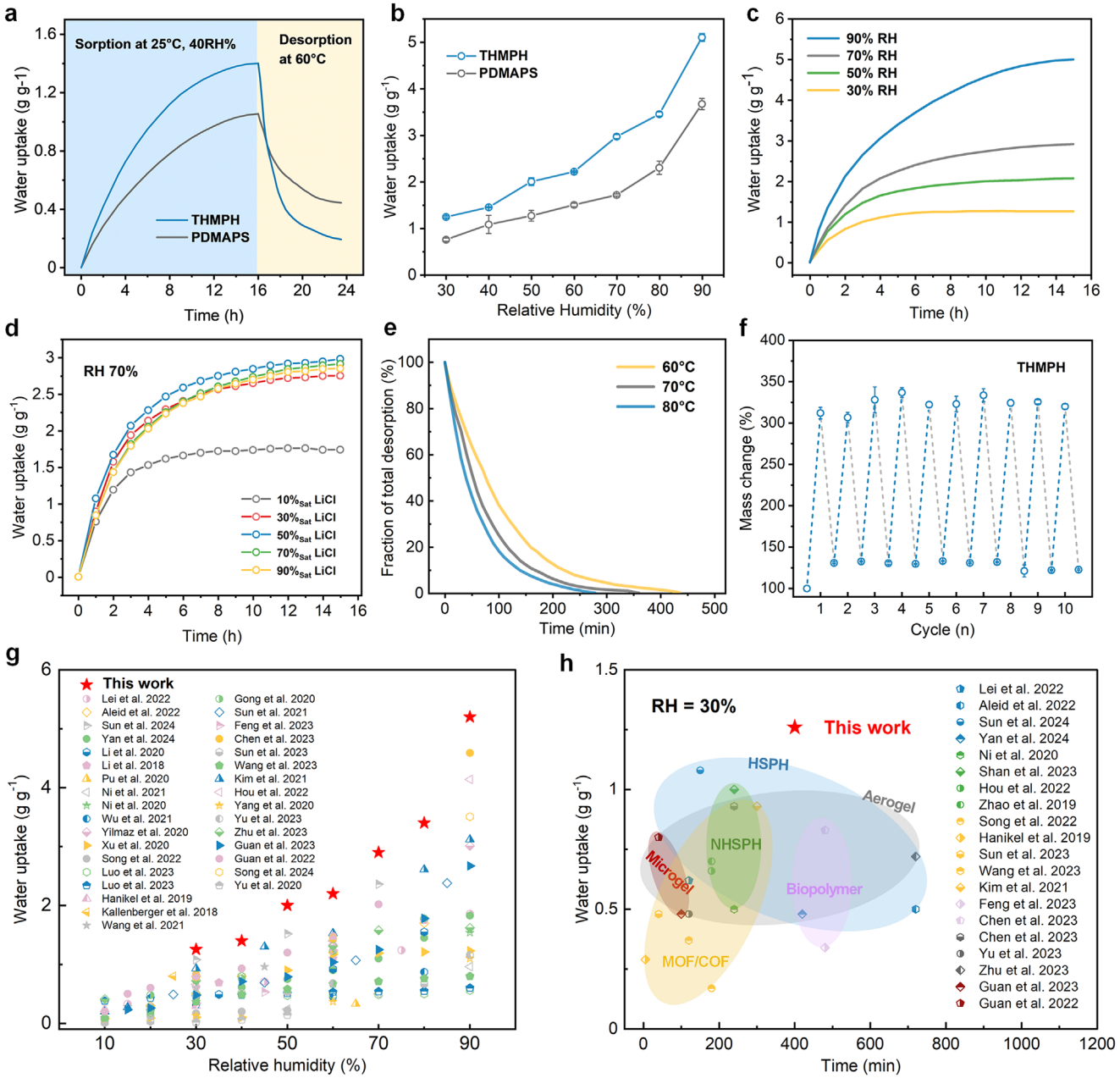


**Figure 3.** Moisture adsorption and desorption performance tests of THMPH and PDMAPS. a) Kinetic curves of water vapor adsorption–desorption process of THMPH and PDMAPS. b) Comparison of moisture adsorption between THMPH and PDMAPS at 25 °C and different relative humidity (from 30% RH to 90% RH). c) Adsorption kinetic curves of THMPH at different humidities. d) The moisture adsorption kinetic curves of THMPH at 25 °C and 70% RH after immersion in different concentrations of LiCl solution. e) Normalized desorption kinetic curves of hydrated THMPH at 60–80 °C, respectively. f) 10 adsorption–desorption cycles were performed for THMPH, with adsorption at 25 °C and 60% relative humidity, and desorption at 90 °C. g) Comparison of water uptake at different RH with other state-of-the-art ASWH. h) Comparison of water uptake and sorption kinetics for THMPH with other state-of-the-art ASWH at 30% RH, including hygroscopic-salt polyelectrolyte hydrogels (HSPH), non-hygroscopic-salt polyelectrolyte hydrogels (NHSPH), MOFs/COFs, biopolymers, aerogels biopolymers, aerogels, microgels and other polymers.

over 24 h, with a theoretical evaporative cooling capacity increase of 1.47 KJ $g^{-1}$. Hygroscopic isotherms of THMPH indicated that under the condition of 30%, 50%, 70%, and 90% RH, the saturated water uptake was 1.2, 2, 2.9, and 5.2 g $g^{-1}$, respectively, exceeding PDMAPS and other SAWH materials (Figure 3b). The rapid hygroscopic kinetics of THMPH also achieved 90% equilibrium within 6 hours across a wide humidity range (Figure 3c,d; Figure S18, Supporting Information). The crosslinking degree during polymerization was influenced by NaCl concentration in the precursor, with higher concentrations resulting in a looser network and preventing over-crosslinking (Figures S19–S21, Supporting Information). The adsorption

kinetic curves of hydrogels soaked in LiCl solutions of different concentrations (Figure 3d) revealed that the 50% saturated LiCl solution achieves the highest loading capacity, leading to the optimal hygroscopic capacity. Excessive LiCl concentration caused pore blockage and osmotic pressure issues, affecting mass transfer, inhibiting LiCl entry into the hydrogel network, and reducing salt loading. Despite this, THMPH achieved a LiCl loading of ≈5 g $g^{-1}$, surpassing PDMAPS under identical conditions (Figures S22–S26, Supporting Information). The hygroscopicity and durability of hydrogels were affected by the leakage of hygroscopic salts. THMPH exhibited minimal LiCl leakage (<2%) after loading in 50% saturated LiCl solution, while PDMAPS lost LiCl up to 50% (Figure S27, Supporting Information). Stable LiCl loading also prevented moisture loss; THMPH maintained stability for over 72 h at 25 °C and 50% RH, whereas LiCl-free hydrogels rapidly dehydrated (Figure S28, Supporting Information). The moisture sorption diffusion coefficient ($D_{ms}$), representing the sorption rate, can be estimated by Fick's second law (Figure S29, Table S3, Supporting Information).

Water desorption tests (Figure 3e) revealed THMPH achieved 90% desorption within 2.5, 3, and 4 h at 60, 70, and 80 °C, respectively, and all finally reaching equilibrium within 7 h, demonstrating rapid desorption performance. The average desorption efficiency (i.e., the ratio of water released to water absorbed) was ≈75%. Cycling stability is demonstrated by the experimental results of capturing and releasing water in 10 adsorption–desorption cycles (Figure 3f). Due to the reduced water release in each cycle, the next water uptake built on the residual water content, so the subsequent water uptake decreases. As expected, an ideal linear fitting between the experimental data and the proposed theoretical mode was observed at 40% RH and 25 °C. THMPH exhibited higher $D_{ms}$ than PDMAPS, demonstrated a better water transfer rate. Figure 3g summarizes the comparative analysis of the moisture absorption capacity of other SAWH materials, including hygroscopic-salt polyelectrolyte hydrogels (HSPH), non-hygroscopic-salt polyelectrolyte hydrogels (NHSPH), MOFs/COFs, biopolymers, aerogels, microgels, and other polymers. THMPH absorbed 1.25 g $g^{-1}$ water within 6 h, indicating better water uptake capacity, and also excelled across a broad humidity range (Figure 3h, Table S4, Supporting Information).

### 2.3. Mechanical Properties of THMPH

SAWH hydrogels often exhibited limited mechanical strength. Uniaxial tensile tests revealed the high toughness (160 kJ $m^{-3}$) and fracture strain (230%) of THMPH, which is seventy and three times that of PDMAPS, respectively. The critical fracture stress was 124.6 kPa and the modulus was 91 kPa, both significantly superior to PDMAPS, attributed to its multi-level crosslinking structure (**Figure 4a**). Weak crosslinks acted as sacrificial bonds, dissipating energy, while strong bonds maintained toughness. Moreover, THMPH retained high strength post-LiCl loading, with only a 30% reduction in tensile strength and strain, due to the stability of the strong crosslinking regions within the THMPH network. In contrast, PDMAPS exhibited an 88% drop in fracture stress and an 80% reduction in strain (Figure 4d; Figures S30–S32, Supporting Information), because the hygroscopic process of PDMAPS is accompanied by the expansion of the polymer network, significantly weakening the mechanical strength. We compared the stress–strain curve under various water contents. THMPH maintained ductility at water contents over 2 g $g^{-1}$, transitioning to brittleness only below 1 g $g^{-1}$ (Figure 4b). At 1 g $g^{-1}$ water uptake, the fracture stress (225 kPa) of THMPH was 200 times higher than PDMAPS (Figure 4c). Even at high water content, THMPH outperformed PDMAPS in strength and toughness.

Similarly, the results of uniaxial static compression tests for the two hydrogels (Figure 4e; Figures S33 and S34, Supporting Information) also showed the difference. The multi-level strong crosslinking network of THMPH resulted in a high yield strength of 285.3 kPa, toughness of 51.3 kJ $m^{-3}$, and a compression modulus of 222 kPa, which were about ten times those of PDMAPS. The physical photos of the two hydrogels during uniaxial compression tests (Figure 4f; Figure S35, Supporting Information) visually demonstrated the differences in mechanical performance between the two hydrogels. Cyclic compression tests (Figure 4g,h; Figure S36, Supporting Information) revealed hysteresis loops for both hydrogels, with THMPH dissipating 11.4 kJ $m^{-3}$ (22.2% of strain energy) compared to 0.84 kJ $m^{-3}$ of PDMAPS (14.3% of strain energy). THMPH exhibited minimal residual strain, indicating efficient energy dissipation via rapidly reversible ionic crosslink breakage. In contrast, PDMAPS showed a yield point at 55% strain, with strength degradation and only 86.2% reversibility after 5 cycles, reflecting significant fatigue behavior. THMPH maintained 98.8% reversibility over 25 cycles at 70% strain (Figure S37, Supporting Information), attributed to its strong–weak synergistic network: weak bonds dissipated energy under stress, while strong bonds preserved structural integrity. After stress unloading, the broken weak crosslinks can quickly reconnect, providing high fatigue resistance. The same trends also in tensile cycling (Figure S38, Supporting Information). Combining high hygroscopicity with exceptional strength, toughness, and reversibility, THMPH surpassed previously reported SAWH materials, including polyzwitterions, polyelectrolytes, and aerogels in performance (Figure 4i).

### 2.4. Evaporative Cooling Performance of THMPH

To verify the effectiveness of THMPH cooling, experiments on PV panels were conducted under simulated sunlight and outdoors, respectively. The cooling performance of the THMPH cooler was verified under simulated sunlight (**Figure 5a**). High temperatures cause irreversible chemical and structural damage to PV cells, which is the main cause of the working life degradation of PV modules. The temperature-dependent degradation process can be explained by the Arrhenius model, which is based on the following equations.

$$k = Ae^{-Ea/RT} \quad (1)$$

$$\frac{K_1}{K2} = e^{\frac{E_a}{R}\left(\frac{1}{T_2}-\frac{1}{T_1}\right)} = AF \quad (2)$$

where $k$ is the rate constant of the process, $A$ is the Arrhenius pre-exponential factor, $E_a$ is the apparent activation energy (J $mol^{-1}$),

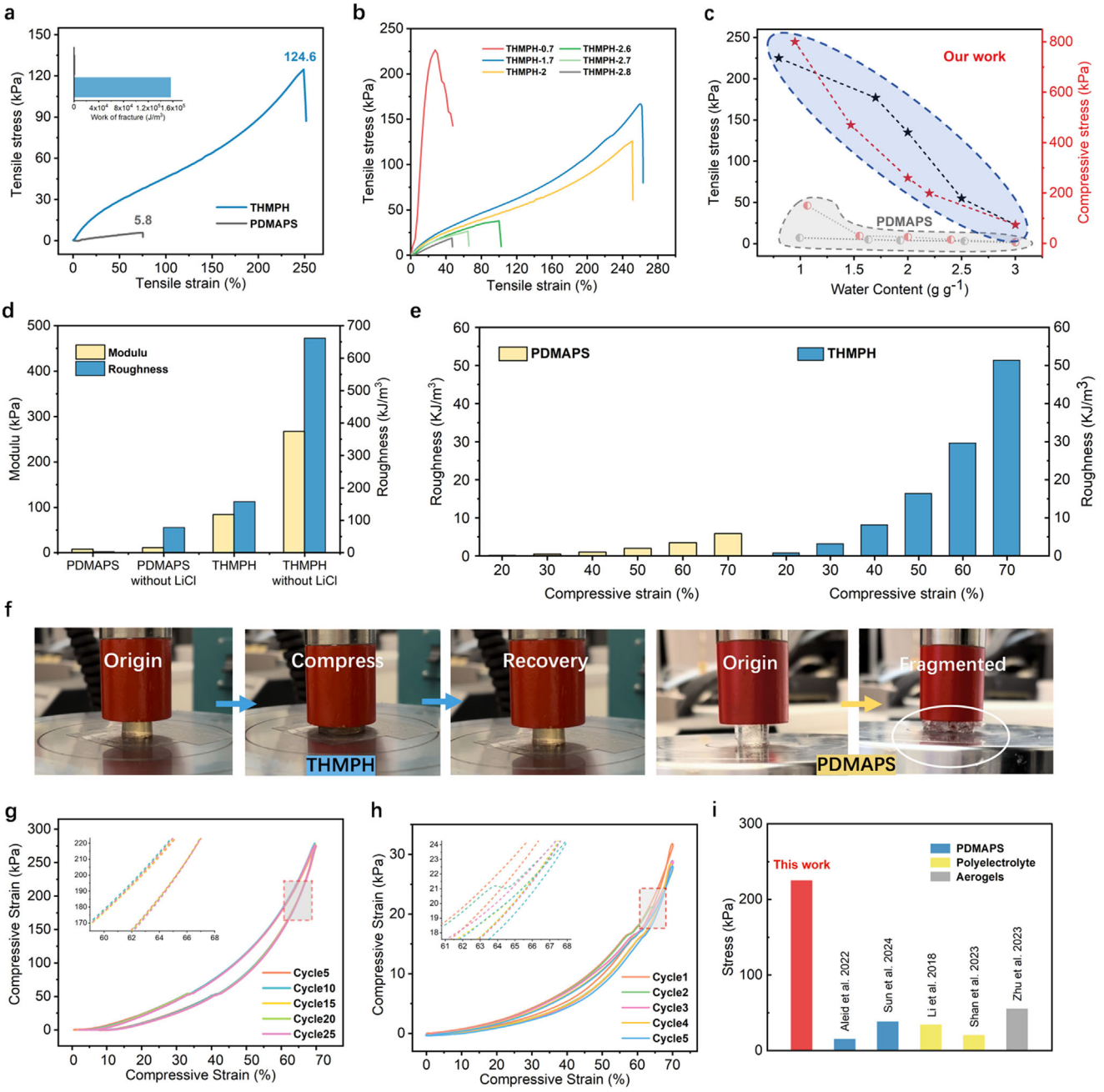


**Figure 4.** Mechanical behaviors of THMPH and PDMAPS. a) Tensile stress–strain curve of THMPH and PDMAPS. b) Tensile stress–strain curves of THMPH at different water contents. c) Comparison of tensile and compressive stresses between THMPH and PDMAPS at different water contents. d) Comparison of toughness and modulus of THMPH and PDMAPS and THMPH and PDMAPS without salt. e) Uniaxial static compression test of THMPH and PDMAPS. f) Physical photographs of THMPH and PDMAPS at 70% compressive strain. Compressive loading–unloading cycles stress–strain curves of g) THMPH and h) PDMAPS. Comparison of tensile stress with other state-of-the-art SAWH strains. i) Comparison of tensile stress with other state-of-the-art SAWH.

$R$ is the gas constant, $T$ is the absolute temperature ($K$), and $AF$ is the accelerating factor for two different test conditions.

Figure 5b shows that the average temperature of photovoltaic cells in operation is ≈65.6 °C; However, with the evaporative cooling module, the average temperature of the cells under the same working conditions dropped to ≈52.5 °C. The cooling hydrogel reduced the operating temperature of the photovoltaic cells by more than 10 °C, leading to an improvement in conversion efficiency (Figures S39–S41, Table S5, Supporting Information). The photovoltaic performance parameters of PV cells demonstrate significant enhancements with decreasing operating temperature, particularly in maximum power output ($P_{max}$), fill factor (FF), and efficiency, with the latter showing a notable increase from 13.58% to 14.64% (Figure 5c).

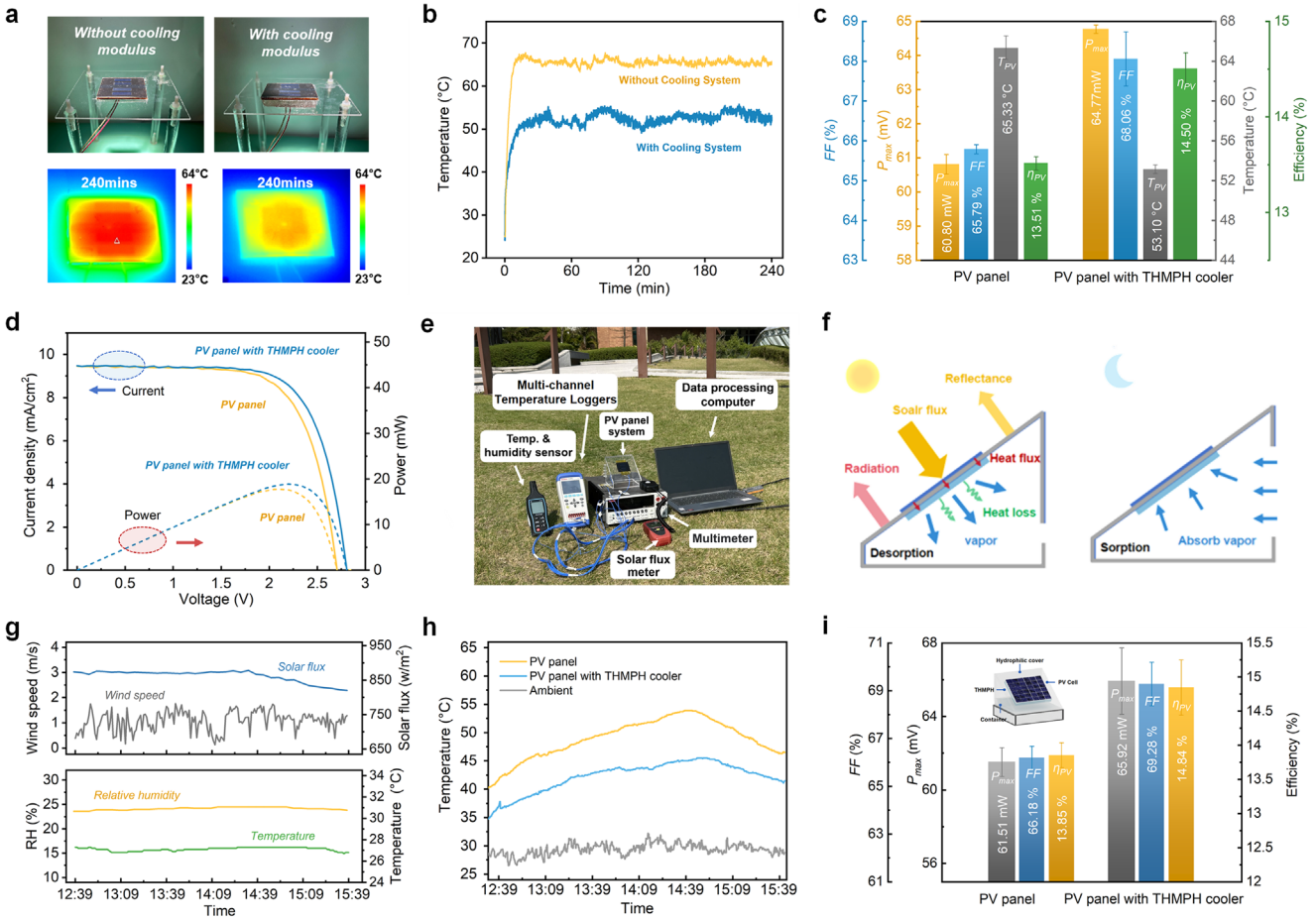


**Figure 5.** Evaporative Cooling system for PV cell and cooling performance of THMPH. a) Images and infrared images for verifying cooling performance under simulated sunlight. b) Surface temperature with and without THMPH cooler in 4 h. c) Maximum power ($P_{max}$), fill factor (FF), temperatures and efficiency ($\eta$), and d) current density and power of the standalone PV panel and PV panel with THMPH cooler. e) Image of the outdoor testing. f) Energy flow diagram of the PV panel module during day and night. g) The solar flux, wind speed, relative humidity, and temperature during outdoor test. h) The working temperature of the PV panel, PV panel with THMPH cooler and ambient temperature. i) $P_{max}$, FF, and efficiency of stable PV panels with and without THMPH cooler modules.

As shown by Figure 5d, the introduction of the cooling hydrogel significantly delayed the performance degradation of photovoltaic cells once the voltage reached 1.5 V. A marked improvement in power output is observed under the same applied voltage. After operating for 240 min with the cooling hydrogel, the current density and voltage curves of the photovoltaic cells were measured, demonstrated exceptional stability. (Figure S42, Supporting Information).

In order to better validate the cooling capability of THMPH on PV cells, we designed a cooling system where a container made of acrylic material is used to hold the PV cells with the cooling module (Figure 5e). The walls of the container were designed to allow the PV cells to receive sunlight better, and a removable back cover was used to absorb atmospheric water vapor from the hydrogel at night. Figure 5f illustrates the energy flow between the PV cells and the cooling module.

The high water content allowed it to dissipate more heat, maintaining efficient operation for up to 12 h to meet daytime cooling demands. Additionally, due to the hydrogel's excellent hygroscopic properties, it can quickly reach saturation at night, ultimately achieving a cycle of atmospheric water collection and evaporative cooling. To evaluate the cooling performance of the hydrogel, the outdoor experiments were conducted from 2:00 to 4:00 PM, exposing the THMPH-based photovoltaic system to sunlight. with an intensity of approximately from 0.6 to 0.9 kW $m^{-2}$. The water absorbed by the hydrogel was gradually evaporated by the heat from the PV panels. Figure 5g illustrates the sun flux, wind speed, ambient temperature, and humidity of the outdoor environment, along with the operational temperature of the photovoltaic cells under these conditions. The results demonstrated that the hydrogel cooling system effectively reduced the average operating temperature, showcasing its stable and efficient cooling performance (Figure 5h). The exceptional cooling performance in outdoor experiments significantly enhances PV cell performance, particularly evidenced by a remarkable 7.33% improvement in efficiency (Figure 5i; Figures S43 and S44, Supporting Information). All-day multicyclic AHW performance of scaled-up THMPH device was also discussed in Figures S45–S51, Table S6 (Supporting Information).

## 3. Conclusion

In summary, this study presents a customizable synthesis strategy for developing novel polyzwitterionic hydrogels, THMPH, which uniquely combine high hygroscopicity with excellent mechanical properties. By comparing with traditional PDMAPS and other highly hygroscopic but relatively brittle SAWHs, this customized polyzwitterionic gel exhibited significantly enhanced mechanical performance while maintaining high hygroscopicity and rapid adsorption kinetics. The exceptional performance of THMPH is a result of strong ionic crosslinking provided by the more stable LiCl loading, enabling higher hygroscopic capacity and rapid water capture and release capabilities. At 30%, 50%, 70%, and 90% RH, it achieved impressive hygroscopic rates of 1.2, 2, 2.9, and 5.2 g $g^{-1}$, respectively, and released 90% of the equilibrium moisture within 2.5 h. Additionally, compared to conventional copolymer chains, the highly stable and strong crosslinking regions interwoven with reversible weak crosslinking bonds in the polymer chain provided excellent strength, elongation, and reversibility. At a water content close to 2 g $g^{-1}$, it can exhibit 230% tensile strain and 124.6 kPa tensile strength. At a water content of 1 g $g^{-1}$, it shows strain strength 200 times higher than polyzwitterion PDMAPS and demonstrates high reversibility without fatigue over more than 25 strain cycles. We further demonstrated the use of THMPH for cyclic atmospheric water harvesting and evaporative cooling in PV cells, significantly enhancing solar conversion efficiency. The novel synthesis strategy reported in this work opens the possibility of widespread applications of SAWH hydrogels, as mechanically robust high-performance SAWH hydrogels can be readily tailored for different application scenarios by simply adjusting the monomer composition. Nonetheless, the inherently variable outdoor environment challenges the maintenance of intimate AWH hydrogel through interfacial instability, uniform heat dissipation, necessitating systematic AWH device investigations, and its expanded applications may need to be further explored.

## 4. Experimental Section

*Materials*: *N*, *N*′- Methylenebis(acrylamide) (BIS) were purchased from Shanghai Aladdin Bio-Chem Technology Co., LTD. Sodium 4-vinylbenzenesulfonate, Sodium chloride, and 3-(methacryloylamino)propyl-trimethylammonium Chloride were all purchased from Shanghai Macklin Biochemical Technology Co., Ltd., [2-(Methacryloyloxy)ethyl]dimethyl-(3-sulfopropyl), 2-oxoglutaric acid, Lithium chloride anhydrous (AR, 99%), and 2-Ketoglutaric acid was purchased from Shenzhen Dieckmann Biotechnology Co., LTD. Deionized Water was purified through a laboratory water purification system.

*Preparation of Polyzwitterionic Hydrogels*: All chemicals were used as purchased without further purification. All chemicals were used as purchased without further purification. NaSS and MPTC with 2.1 M ionic monomer concentration, 0.4 mol% BIS as cross-linker content, 0.5MNaCl, and 0.25 mol% of -Ketoglutaric acid as photoinitiator were mixed with deionized water with an anionic monomer molar fraction of 0.52. The mixed solution containing NaSS monomer and MPTC monomer was then poured into a glass mold and irradiated with a 365 nm UV lamp for 10 h to obtain the poly(amphoteric) hydrogel. Afterward, the prepared hydrogels were immersed in a large amount of deionized water for 24 h to wash off the residues. The reaction kinetics confirmed the random copolymerization of anionic and cationic monomers in the hydrogels. In order to prepare hydrogels with the addition of hygroscopic salts of LiCl, the prepared samples were dried in an oven at 90 °C for more than 12 h, and then the dried samples were immersed into LiCl solutions with different solid contents until the weight was stable. Then the dried samples were immersed in LiCl solutions with different solid contents (10, 30, 50, 70, and 90 wt.%$_{sat}$) until the weight was stabilized. The prepared NaSS/MPTC hydrogel was named THMPH. DMAPS was polymerized with the same cross-linker concentration and monomer concentration, and the prepared hydrogel was named PDMAPS.

*Characterizations*: Scanning electron microscopy images were taken using a Cryo-SEM Bio-Cryo Scanning Electron Microscope to observe the morphology and microstructure of the hydrogels in the hydrated state. The spectral range of the spectrum-two FTIR of PerkinElmer, USA was 4000–500 $cm^{-1}$, and the gels were prepared with a size of 3 cm × 1 cm, and each sample was scanned 16 times. TGA was carried out by a thermogravimetric analyzer (PerkinElmer, TGA 4000), and the hydrogels were heated up in the range of 30–650 °C with an airflow rate of 25 mL $min^{-1}$ and a heating rate of 5 °C $min^{-1}$. The static absorbency and stability tests of the hydrogels were performed at room temperature. The prepared samples were dried in an oven at 90 °C and the weights were recorded, and then the samples were put into a large amount of deionized water, and the final weights of the hydrogels were recorded after there was no change in the mass. After that, the hydrogels were placed in a constant temperature and humidity environment (25 °C, relative humidity = 60%) to observe the change in the quality of the hydrogels. Atmospheric water harvesting was performed to characterize the hydrogel's ability to automatically capture atmospheric water molecules, that is, the rate of water absorption and the amount of water absorbed. The hydrogels with consistent specifications were dried in an oven at 90 °C for at least 12 h. The dried samples were then placed in an environmental chamber where the temperature and humidity were varied according to the experimental conditions, and the changes in the mass of the hydrogels were recorded continuously with an electronic balance.

## Supporting Information

Supporting Information is available from the Wiley Online Library or from the author.

## Acknowledgements

This research was financially supported by the GRF grant: # 15204023 from the Hong Kong Research Council, Seed Fund project: BBFH from PolyU Research Centre of Textiles as well as Postdoc Matching Fund Project: W36P from Hong Kong Polytechnic University. Meanwhile, the authors would like to acknowledge the facility support provided by the University of Texas at Austin.

## Conflict of Interest

The authors declare no conflict of interest.

## Data Availability Statement

The data that support the findings of this study are available from the corresponding author upon reasonable request.

## Keywords

atmospheric water harvesting, energy conversion efficiency, evaporative cooling, mechanical robustness, mix-charged polyzwitterionic hydrogels

Received: March 18, 2025
Revised: May 10, 2025
Published online: May 30, 2025

[1] E. R. Jones, M. F. P. Bierkens, M. T. H. van Vliet, *Nat. Clim. Change* **2024**, *14*, 629.
[2] R. K. Mishra, *BJMAS* **2023**, *4*, 208.
[3] M. M. Mekonnen, A. Y. Hoekstra, *Sci. Adv.* **2016**, *2*, 1500323.
[4] M. J. Kalmutzki, C. S. Diercks, O. M. Yaghi, *Adv. Mater.* **2018**, *30*, 1704304.
[5] H. Lu, W. Shi, Y. Guo, W. Guan, C. Lei, G. Yu, *Adv. Mater.* **2022**, *34*, 2110079.
[6] E. Radziemska, *Renewable Energy* **2003**, *28*, 1.
[7] A. Jäger-Waldau, *EPJ Photovoltaics* **2023**, *14*, 23.
[8] R. Li, Y. Shi, M. Wu, S. Hong, P. Wang, *Nat. Sustainability* **2020**, *3*, 636.
[9] A. Makki, S. Omer, H. Sabir, *Renewable Sustainable Energy Rev.* **2015**, *41*, 658.
[10] F. Luo, X. Liang, W. Chen, S. Wang, X. Gao, Z. Zhang, Y. Fang, *Small* **2023**, *19*, 2304477.
[11] F. Luo, X. Liang, W. Chen, S. Wang, X. Gao, Z. Zhang, Y. Fang, *Chem. Eng. J.* **2023**, *465*, 142891.
[12] Y. Song, N. Xu, G. Liu, H. Qi, W. Zhao, B. Zhu, L. Zhou, J. Zhu, *Nat. Nanotechnol.* **2022**, *17*, 857.
[13] N. Hanikel, M. S. Prévot, F. Fathieh, E. A. Kapustin, H. Lyu, H. Wang, N. J. Diercks, T. G. Glover, O. M. Yaghi, *ACS Cent. Sci.* **2019**, *5*, 1699.
[14] Y. Wang, W. Chen, J. Fu, Y. Liu, *eScience* **2023**, *3*, 100154.
[15] C. Sun, Y. Zhu, P. Shao, L. Chen, X. Huang, S. Zhao, D. Ma, X. Jing, B. Wang, X. Feng, *Angew. Chem., Int. Ed.* **2023**, *62*, 202217103.
[16] D. Zhu, H. Wu, S. Wang, *Int. J. Therm. Sci.* **2006**, *45*, 804.
[17] H. Zhao, Z. Wang, Q. Li, T. Wu, M. Zhang, Q. Shi, *Micropor. Mesopor. Mater.* **2020**, *299*, 110109.
[18] W. Shi, W. Guan, C. Lei, G. Yu, *Angew. Chem.* **2022**, *134*, 202211267.
[19] A. S. Mohammed Ali, H. M. Hegab, F. Almarzooqi, M. A. Jaoude, S. W. Hasan, F. Banat, *J. Environ. Chem. Eng.* **2024**, *12*, 113319.
[20] A. Heidari, R. Roshandel, V. Vakiloroaya, *Energy Convers. Manage.* **2019**, *185*, 396.
[21] H. Maher, T. H. Rupam, K. A. Rocky, R. Bassiouny, B. B. Saha, *Energy* **2022**, *238*, 121741.
[22] R. Li, Y. Shi, L. Shi, M. Alsaedi, P. Wang, *Environ. Sci. Technol.* **2018**, *52*, 5398.
[23] S. K. Sibie, M. F. El-Amin, S. Sun, *Energies* **2021**, *14*, 3822.
[24] L. Guo, W. Gu, C. Peng, W. Wang, Y. J. Li, T. Zong, Y. Tang, Z. Wu, Q. Lin, M. Ge, G. Zhang, M. Hu, X. Bi, X. Wang, M. Tang, *Atmos. Chem. Phys.* **2019**, *19*, 2115.
[25] Y.-T. Li, H. Chen, R. Deng, M.-B. Wu, H.-C. Yang, S. B. Darling, *ACS Appl. Mater. Interfaces* **2021**, *13*, 33713.
[26] R. Li, Y. Shi, M. Wu, S. Hong, P. Wang, *Nano Energy* **2020**, *67*, 104255.
[27] H. Shan, Q. Pan, C. Xiang, P. Poredoš, Q. Ma, Z. Ye, G. Hou, R. Wang, *Cell Rep. Phys. Sci.* **2021**, *2*, 100664.
[28] J. Sun, F. Ni, J. Gu, M. Si, D. Liu, C. Zhang, X. Shui, P. Xiao, T. Chen, *Adv. Mater.* **2024**, *36*, 2314175.
[29] C. Lei, Y. Guo, W. Guan, H. Lu, W. Shi, G. Yu, *Angew. Chem., Int. Ed.* **2022**, *61*, 202200271.
[30] M. Song, T. Cheng, Y. Li, D. Huang, X. Huang, H. Xie, L. Wang, Y. Yue, W. Yu, *J. Cleaner Prod.* **2024**, *461*, 142661.
[31] M. Dai, F. Zhao, J. Fan, Q. Li, Y. Yang, Z. Fan, S. Ling, H. Yu, S. Liu, J. Li, W. Chen, G. Yu, *Adv. Mater.* **2022**, *34*, 2200865.
[32] Y. Zhang, L. Wu, X. Wang, J. Yu, B. Ding, *Nat. Commun.* **2020**, *11*, 3302.
[33] S. Pu, Y. Liao, K. Chen, J. Fu, S. Zhang, L. Ge, G. Conta, S. Bouzarif, T. Cheng, X. Hu, K. Liu, J. Chen, *Nano Lett.* **2020**, *20*, 3791.
[34] X. Zhou, P. Zhang, F. Zhao, G. Yu, *ACS Mater. Lett.* **2020**, *2*, 1419.
[35] H. Itagaki, T. Kurokawa, H. Furukawa, T. Nakajima, Y. Katsumoto, J. P. Gong, *Macromolecules* **2010**, *43*, 9495.
[36] H. Shan, P. Poredoš, Z. Ye, H. Qu, Y. Zhang, M. Zhou, R. Wang, S. C. Tan, *Adv. Mater.* **2023**, *35*, 2302038.
[37] R. Li, Y. Shi, M. Alsaedi, M. Wu, L. Shi, P. Wang, *Environ. Sci. Technol.* **2018**, *52*, 11367.
[38] S. Aleid, M. Wu, R. Li, W. Wang, C. Zhang, L. Zhang, P. Wang, *ACS Mater. Lett.* **2022**, *4*, 511.
[39] Y. Hou, Z. Sheng, C. Fu, J. Kong, X. Zhang, *Nat. Commun.* **2022**, *13*, 1227.
[40] K. Shah, D. Vasileva, A. Karadaghy, S. P. Zustiak, *J. Mater. Chem. B* **2015**, *3*, 7950.
[41] M. Imaninezhad, I. Kuljanishvili, S. P. Zustiak, *Macromol. Biosci.* **2017**, *17*, 1600261.
[42] A. A. Adewunmi, S. Ismail, A. S. Sultan, *J. Inorg. Organomet. Polym. Mater.* **2016**, *26*, 717.
[43] L. Zhao, Z. Yang, J. Wang, Y. Zhou, P. Cao, J. Zhang, P. Yuan, Y. Zhang, Q. Li, *Chem. Eng. J.* **2023**, *451*, 138676.
[44] P. Zhu, Z. Yu, H. Sun, D. Zheng, Y. Zheng, Y. Qian, Y. Wei, J. Lee, S. Srebnik, W. Chen, G. Chen, F. Jiang, *Adv. Mater.* **2024**, *36*, 2306653.
[45] D. Zhong, Z. Wang, J. Xu, J. Liu, R. Xiao, S. Qu, W. Yang, *Nat. Commun.* **2024**, *15*, 5896.
[46] R. Zhu, D. Zhu, Z. Zheng, X. Wang, *Nat. Commun.* **2024**, *15*, 1344.
[47] J. Kim, G. Zhang, M. Shi, Z. Suo, *Science* **2021**, *374*, 212.
[48] J. Wittmer, A. Johner, J. F. Joanny, *Europhys. Lett.* **1993**, *24*, 263.
[49] S. Kim, N. Lee, Y. Jung, A. Johner, *Polymers* **2024**, *16*, 2928.
[50] P. G. Higgs, J.-F. Joanny, *J. Chem. Phys.* **1991**, *94*, 1543.